Desalination and Water Treatment
www.deswater.com

doi: 10.5004/dwt.2022.28616

266 (2022) 256–267
August

Removal of triclosan from aqueous solution using biochar derived from seed shell of *Aesculus turbinata*

Eun-Ji Cho[a], Joon-Kwan Moon[b], Chang-Gu Lee[c], Seong-Jik Park[a,d,*]

[a]*Department of Bioresources and Rural Systems Engineering, Hankyong National University, Anseong 17579, Republic of Korea, Fax: +82-31-670-5139; email: parkseongjik@hknu.ac.kr (S.-J. Park), ORCID: 0000-0003-2122-5498*
[b]*Department of Plant and Environmental Science, Hankyong National University, Anseong 17579, Republic of Korea*
[c]*Department of Environmental and Safety Engineering, Ajou University, Suwon 16499, Republic of Korea*
[d]*Institute of Agricultural Environmental Sciences, Hankyong National University, Anseong 17579, Republic of Korea*

Received 22 November 2021; Accepted 3 June 2022

ABSTRACT

The applicability of biochar derived from *Aesculus turbinata* seed shell (SAT-BC) was investigated for triclosan removal, which is extensively used in personal care products and causes endocrine disorders. The seed shells were pyrolyzed at 300°C–700°C, and their physico-chemical properties and triclosan adsorption capacities were analyzed. The increase in pyrolysis temperature from 300°C to 700°C decreased the O/C and H/C of SAT-BC from 0.205 to 0.130 and from 0.071 to 0.021, respectively. SAT-BC at 300°C (SAT-300) presented a higher triclosan adsorption capacity than that of SAT-BC pyrolyzed at other temperatures. Adsorption equilibrium was achieved at a reaction time of 6 h, and the pseudo-second-order model better fit the triclosan adsorption by SAT-300. The equilibrium adsorption data was best represented by the Freundlich isotherm model, and the maximum adsorption capacity was estimated to be 49.4 mg/g. The enthalpy and entropy change during triclosan adsorption by SAT-BC were 22.2 kJ/mol and 67.9 J/K·mol, respectively, indicating that the triclosan adsorption absorbed energy and increased the randomness during the processes. The increase of solution pH from 3 to 11 decreased triclosan adsorption from 33.0 to 7.4 mg/g, and a sharp drop in adsorption amount (23.5–14.6 mg/g) was observed between solutions pH 7 and 9. Increasing the SAT-300 dose from 1.7 to 10.0 g/L decreased the triclosan adsorption per unit mass of adsorbent, but increased the removal percentage; 8.3 g/L of the adsorbent dose removed more than 90% of triclosan. The biowaste turbinate seed shell pyrolyzed at 300°C can be potentially used for triclosan adsorption.

Keywords: Triclosan; Biochar; Pyrolysis temperature; *Aesculus turbinata*; Hydrogen bonding; Elemental composition

1. Introduction

Triclosan (5-chloro-2-(2,4-dichlorophenoxy)phenol), an antimicrobial agent that offers an immediate and broad-spectrum antimicrobial activity, is found in consumer products such as soap, deodorants, lotions, toothpaste, and hand and body wash [1]. According to previous studies, personal care products contain 0.1%–0.3% of triclosan, which enter the wastewater treatment facilities [2]. The global concentration of triclosan ranges from 1.4 to 40,000 ng/L; due to its incomplete removal from wastewater treatment plants, it continues to flow into aquatic environments such as seas, lakes, and rivers [3,4]. Triclosan and its by-products have been recently reported to cause problems such as microbial resistance, skin irritation, endocrine disorders, an increased incidence of allergies, changes in thyroid hormone metabolism, and tumor development [5]. Trace amounts of triclosan can be detrimental to aquatic organisms such as algae, invertebrates, and fish [6]. Triclosan has been repeatedly detected in both the influent and effluent

* Corresponding author.

of wastewater treatment plants, and low-level triclosan removal and runoff are particularly problematic in wastewater treatment with short residence time, such as trickling filters [7].

In recent studies, various techniques have been explored for removing triclosan from water or aqueous media. Methods such as chlorination, ozonation, Fenton treatment, and electrochemical oxidation that have been used for triclosan treatment require relatively advanced technology and high cost [8]. Adsorption, the interactions between the adsorbate and adsorbent due to various sites and moieties on the adsorbent [9], has been widely applied in triclosan removal [10]. This is because adsorption produces less secondary pollution to the environment and does not require a high cost of construction and operation, energy, or highly skilled operation [9,11,12]. Activated carbon and carbon nanotubes exhibit increased efficiency in the removal of triclosan [13,14]. In particular, activated carbon has well-formed pores and a large surface area; therefore, it is effective in removing small organic compounds [15,16]. However, this material has a relatively high cost, which poses a challenge in removing micro-contaminants on a large scale [13]. Thus, biochar is used as an alternative to activated carbon because of its ability to function as an effective and inexpensive adsorbent for removing micro-contaminants [17].

Biochar, a carbon-rich by-product produced by the thermochemical conversion of various biomass types, has been used in various fields, including as an adsorbent for remediating contaminated soil and water [18,19]. The feedstock to produce biochar include wood, industrial waste, activated sludge, and lignocellulosic biomass, and their properties can be altered depending on the pyrolysis temperature and treatment time [18]. Lignin is a carbon-rich material, and researchers have reported that biochar manufactured from lignin-containing biomass can be used to remove aromatic contaminants [20,21]. *Aesculus turbinata* is a plant in Hippocastanaceae family, and its fruits mainly contain carbohydrates, in addition to lignin, cellulose, and proteins [22,23]. *A. turbinata* seeds have been used as a valuable food resource since ancient times and have been regarded as a food preservative because of their long storage characteristics [24]. A recent study revealed that *A. turbinata* seeds contains saponins, which effectively attenuate an increase in blood glucose levels and fat digestion in vivo [25]. Further research on using the biowaste, that is, shells after the use of seeds is required. To our best knowledge, the researchers have never tried to apply biochars derived from the *A. turbinata* seed shell (SAT-BC) as an adsorbent for removing triclosan from an aqueous solution.

This is the first study to investigate the applicability of SAT-BC for triclosan removal, and the chemical/physical properties and triclosan adsorption capacity of SAT-BC were analyzed to confirm their characteristics as adsorbents. Furthermore, the relationship between the physico-chemical properties and triclosan removal capacity of SAT-BC pyrolyzed at different temperatures was evaluated. Kinetic, equilibrium, and thermodynamic adsorption experiments, and mathematical model analysis were performed to quantify triclosan removal by SAT-BC and investigate its adsorption mechanism. The effect of the solution pH and various doses of SAT-BC on triclosan adsorption were also studied.

2. Materials and methods

2.1. Chemicals

Triclosan (≥97%) was purchased from Sigma-Aldrich (USA), and stock solution (200 mg/L) was prepared by dissolving 200 mg triclosan in a mixture containing 0.2 L of high-performance liquid chromatography (HPLC) grade acetonitrile (Samchun, Korea) and 0.8 L of deionized water. The stock solution was stored in a dark bottle to inhibit photodegradation loss and used within a month. A standard solution of the desired concentration was prepared by diluting the stock with 20% acetonitrile in deionized water. HCl (Samchun, Korea) and NaOH (Samchun, Korea) reagents were used to adjust the pH.

2.2. Preparation of biochar derived from A. turbinata seed shell

The seed shell of *A. turbinata* used in this study was collected from the campus of Hankyong National University, Anseong, Korea. All impurities from the material surface of the seed shell was removed using deionized water. After washing, the seed shell was oven-dried at 80°C for 24 h to remove moisture. The prepared seed shells (15 g) were injected for each batch and pyrolyzed using a muffle furnace with a stainless-steel tube (5.5 cm diameter × 55 cm length). Pyrolysis was performed for 1 h under different temperatures (300°C, 400°C, 500°C, 600°C, and 700°C) at a heating rate of 25°C/min, and nitrogen with a purity of >99.9% was injected to the furnace at a rate of 0.5 L/min to maintain anoxic conditions.

2.3. Characterization of biochar

The physical and chemical characteristics of the raw seed shells (SAT-Raw), and the seed shell biochar pyrolyzed at 300°C, 400°C, 500°C, 600°C, and 700°C (SAT-300, SAT-400, SAT-500, SAT-600, and SAT-700, respectively) were analyzed and studied. The functional groups on the seed shell were analyzed using Fourier-transform infrared spectroscopy (FTIR; Nicolet 6700, Thermo Fisher Scientific, United Kingdom). The surface morphology and chemical element composition of the seed shell were analyzed using field-emission scanning electron microscopy (FE-SEM; S-4700, Hitachi, Japan) and an energy-dispersive X-ray spectrometer (EDS) attached to FE-SEM, respectively. The contents of C, H, N, and S were measured using an automatic elemental analyzer (EA, Flash Smart, Thermo Fisher, USA). A surface area analyzer (Quadrasorb SI, Quantachrome Instruments, USA) was employed to measure the specific surface area, pore volume, and pore diameter of the SAT-BC pyrolyzed at different temperatures. The obtained N_2 adsorption–desorption isotherm curves were analyzed using the Brunauer–Emmett–Teller (BET) equations. Thermogravimetric analysis (TGA) was conducted using a thermogravimetric analyzer (Pyris1, PerkinElmer, USA) under N_2 injection and the mass change of the seed shell was observed as the temperature increased from 25°C to 800°C.

2.4. Triclosan removal experiment

The batch experiment for triclosan adsorption by SAT-BC at various temperatures was performed by treating

30 mL of 100 mg/L triclosan solution with 0.05 g of each adsorbent. The resulting mixtures were stirred at 25°C for 24 h at 100 rpm in a thermostatic shaking incubator (SJ-808SF, Sejong Science, Korea). In all subsequent batch experiments, the temperature and stirring speed of the shaking incubator were constantly maintained. After the reaction, all samples were filtered using glass microfiber filters (Whatman, USA) to separate the adsorbent from the triclosan solution. A Luna C18(2) column and a UV-visible detector included in the HPLC (LC-20AD, Shimadzu, Japan) unit were used to quantify triclosan concentration at a wavelength of 280 nm [26–28]. Acetonitrile/trifluoroacetic acid (0.1%) was used as the mobile phase, and the flow rate of the eluent was 0.8 mL/min. The sample (10 μL) was injected for analysis, and the column temperature was maintained at 30°C. For quantification purposes, standard curves were obtained for the experimental concentration ranges (coefficient of determination, $R^2 > 0.99$). All experiments were conducted thrice, and the averages of the experimental values were calculated and used for analysis.

Triclosan adsorption kinetics for SAT-300 was performed using an initial triclosan concentration of 100 mg/L, and experiments were performed at different reaction times from 0.25 to 12 h. Thereafter, all reactions were performed by combining 0.05 g SAT-300 with 0.03 L of 100 mg/L triclosan solution and reacting at 25°C for 12 h, unless otherwise specified. The equilibrium of triclosan adsorption on SAT-300 was performed using different initial triclosan concentrations (5–100 mg/L) with 0.02 g SAT-300, and mixtures of 0.02 g SAT-300 and 30 mL of triclosan solution at each concentration were reacted for 12 h. SAT-300-mediated triclosan adsorption was performed at different pH conditions of 3–11. The pH of the 100 mg/L triclosan solution was adjusted by adding 0.1 M NaOH or 0.1 M HCl solution, and the initial and final pH was measured using a pH meter (SevenMulti S40; Mettler Toledo, Switzerland). Triclosan adsorption using different doses of SAT-300 (0.05, 0.1, 0.15, 0.2, 0.25, and 0.3 g) was also conducted by reacting with a fixed volume (30 mL) of 100 mg/L triclosan solution. Thermodynamic adsorption experiments were performed by varying the reaction temperature to 15°C, 25°C, and 35°C under similar experimental conditions, except at the designated temperatures.

2.5. Data analysis

The kinetic data were analyzed using pseudo-first-order [Eq. (1)], pseudo-second-order [Eq. (2)], and intraparticle diffusion [Eq. (3)] models, and the equations are as follows:

$$q_t = q_e\left(1 - e^{-k_1 t}\right) \tag{1}$$

$$q_t = \frac{k_2 q_e^2 t}{1 + k_2 q_e t} \tag{2}$$

$$q_t = K_p t^{1/2} + C_p \tag{3}$$

where q_t is the amount of triclosan adsorbed at time t (mg/g), q_e is the amount of triclosan adsorbed onto SAT-300 at equilibrium (mg/g), k_1 is the rate constant of pseudo-first-order adsorption (h^{-1}), and k_2 is the rate constant of pseudo-second-order adsorption (g/mg/h). In Eq. (3), C_p is the intercept (mg/g), and K_p is the intraparticle diffusion rate constant (mg/g·$h^{1/2}$).

The equilibrium data were analyzed using Langmuir [Eq. (4)] and Freundlich [Eq. (5)] isotherm models, and the equations are as follows:

$$q_e = \frac{Q_m K_L C_e}{1 + K_L C_e} \tag{4}$$

$$q_e = K_F C_e^{1/n} \tag{5}$$

where C_e is the triclosan concentration in the aqueous solution at equilibrium (mg/L), K_L is the Langmuir constant related to the binding energy (L/mg), Q_m is the maximum adsorption capacity of triclosan removed per unit mass of SAT-300 (mg/g), K_F is the Freundlich isotherm constant, and ((mg/g)·$(L/mg)^{1/n}$) and $1/n$ is the adsorption intensity. The values of K_L, Q_m, K_F, and n were determined by fitting the experimental data to the Langmuir and Freundlich models. All parameters of the models were measured by nonlinear regression using the Dynamic Fit Wizard function of Sigma-Plot 10.0.

The thermodynamic properties of the experimental results were analyzed using the following equations:

$$\Delta G^\circ = \Delta H^\circ - T\Delta S^\circ \tag{6}$$

$$\Delta G^\circ = -RT \ln K_e \tag{7}$$

$$\ln K_e = \frac{\Delta S^\circ}{R} - \frac{\Delta H^\circ}{RT} \tag{8}$$

$$K_e = \frac{\alpha q_e}{C_e} \tag{9}$$

where ΔG° is the change in Gibb's free energy (kJ/mol), ΔS° is the change in entropy (J/mol·K), ΔH° is the change in enthalpy (kJ/mol), R is the ideal gas constant (J/mol·K), K_e is the equilibrium constant (–), and α is the amount of adsorbent dose (g/L).

3. Results and discussion

3.1. Characterization of A. turbinata seed shell pyrolyzed under different temperatures

The physical and chemical composition of SAT-BC pyrolyzed at different temperatures were characterized. Fig. 1 shows the surface morphologies of the SAT-BC obtained using FE-SEM. The SAT-BC surface became coarser and disintegrated into debris with the increase in pyrolysis temperature. The low specific surface area of raw *A. turbinata* did not observe substantial change during heat treatment (i.e., pyrolysis). This result is inconsistent with the literature,

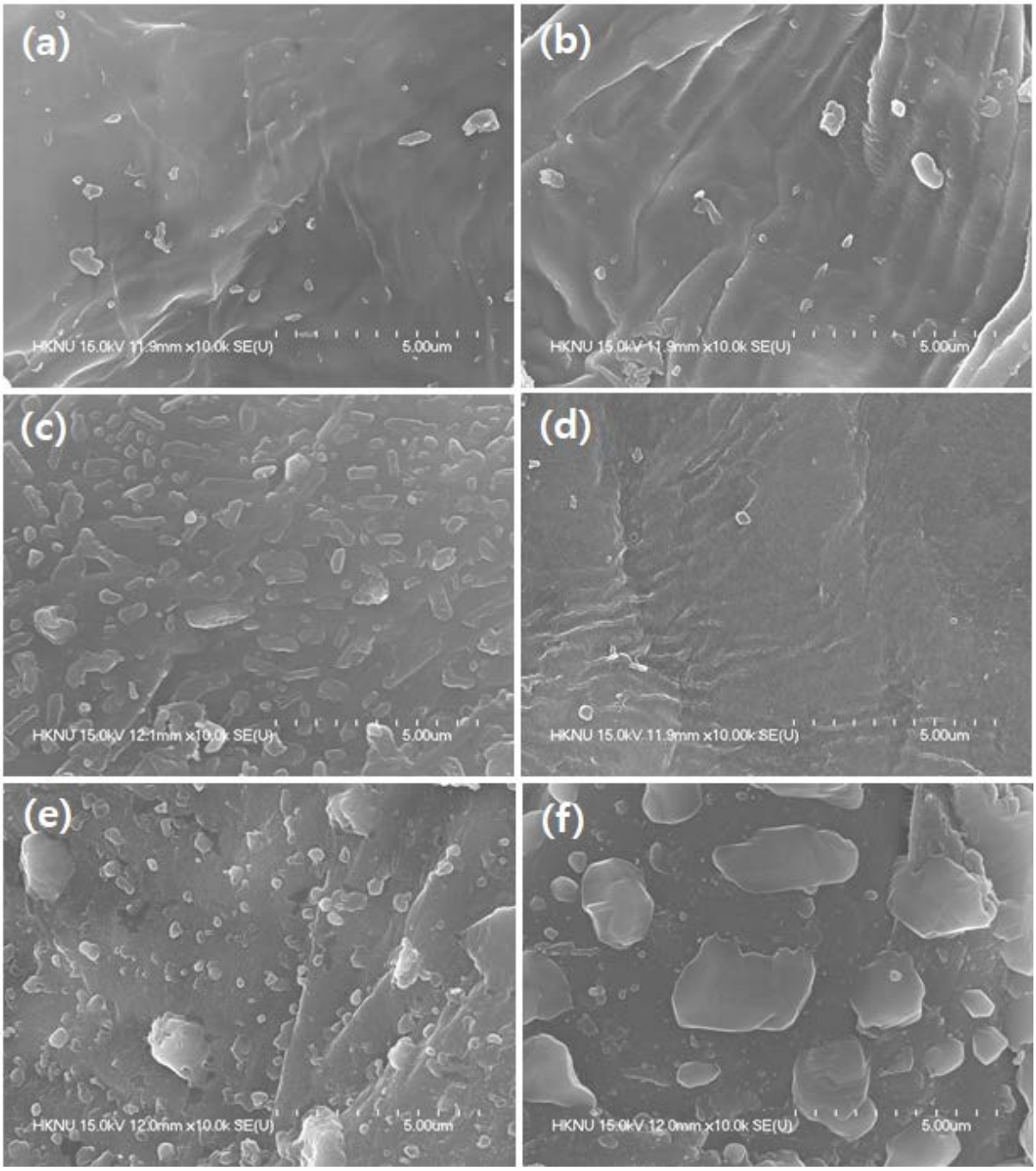

Fig. 1. FE-SEM images of biochar derived from *Aesculus turbinata* seed shells at different temperatures. (a) Non-treated seed shell, (b) biochar derived from seed shell at 300°C (SAT-300), (c) 400°C, (d) 500°C, (e) 600°C, and (f) 700°C.

where an increase in temperature can form larger pores on the biochar and increase its specific surface area [29]; but excessive pyrolysis temperature can reduce the specific surface area because of particle shrinkage and pore sealing [30]. Biochar pores are classified into micropores (<2 nm), mesopores (2–50 nm), and macropores (>50 nm) according to their pore size [31]. As shown in Table 1, SAT-BC was mainly composed of mesopores and macropores.

The chemical compositions of SAT-BC at different temperatures were obtained from EDS analysis and EA, and the results are presented in Table 1. SAT-BC was mainly composed of C, O, K, and H, and their percentages differed depending on the pyrolysis temperature. Although elemental analysis using EA was performed to measure the C, H, N, and S contents of SAT-BC, N and S were not detected. The EDS and EA results revealed that the C content of SAT-BC increased, but the O and H contents decreased as the pyrolysis temperature increased. The increase in pyrolysis temperature from non-treatment to 700°C decreased the O/C ratio from 0.360 to 0.130, indicating a

Table 1
Specific surface area, pore structure, and elemental composition of *Aesculus turbinata* seed shell-derived biochar under different temperatures

Pyrolysis temperature (°C)	Elemental composition (weight %)[a]				Pore structure			Elemental composition (weight %)[b]			pH
	C	O	K	O/C	Specific surface area (m^2/g)	Pore volume (cm^3/g)	Pore size (nm)	C	H	H/C	
Non-treated	69.7 ±0.6	25.1 ±0.6	5.1 ±0.3	0.360	2.25	0.0067	59.7	42.8 ±0.2	5.6 ±0.1	0.130	5.94[c] 6.53[d]
300	79.9 ±5.2	16.4 ±3.1	3.7 ±1.9	0.205	2.02	0.0059	11.6	57.3 ±0.2	4.1 ±0.2	0.071	8.36 8.29
400	78.6 ±0.5	15.6 ±0.7	5.8 ±1.3	0.198	1.44	0.0047	13.0	61.7 ±1.2	3.4 ±0.1	0.055	9.50 8.56
500	82.1 ±2.4	12.8 ±3.1	5.2 ±1.6	0.156	2.10	0.0062	59.2	65.6 ±0.8	2.8 ±0.0	0.043	9.89 9.36
600	80.0 ±0.1	12.1 ±1.8	8.0 ±1.5	0.151	2.11	0.0062	11.8	66.9 ±0.9	1.7 ±0.1	0.026	9.75 9.48
700	82.6 ±1.5	10.8 ±2.2	6.1 ±2.5	0.130	1.39	0.0068	19.7	65.9 ±2.8	1.4 ±0.1	0.021	9.75 9.77

[a]Elemental composition obtained from an energy-dispersive spectrometer;
[b]Elemental composition obtained using an elemental analyser;
[c]Upper pH value obtained from the reaction with deionized water;
[d]Lower pH value obtained from reaction with triclosan solution (100 mg/L).

decrease in the hydrophilicity of the biochar surface [32]. A reduction in the O/C ratio by increasing the pyrolysis temperature also promoted the degree of carbonization [33]. An increase in the pyrolysis temperature from non-treated to 700°C resulted in a decrease in the H/C ratio from 0.130 to 0.021. The H/C ratio is an index of aromaticity, and smaller the value, the higher the aromaticity of the biochar [34]. The low H/C and O/C ratios obtained at high pyrolysis temperatures indicate that the carbon in the biochar was unsaturated [35]. Thus, as the pyrolysis temperature increased, the aromaticity increased, and the hydrophilicity and polarity decreased [36].

Fig. 2a shows the ATR-FTIR spectra and compares the evolution of the SAT-BC pyrolyzed at different temperatures. Various peaks were observed for the SAT-Raw. The observed peak in the region of 3,300 cm^{-1} is due to –OH stretching, which emerges because of adsorbed water molecules, hydroxyl, and carboxylic acid functional groups, and disappears after pyrolysis [37]. The maximum peak at 1,030 cm^{-1} in SAT-Raw represents C–O stretching of cellulose, hemicellulose, and lignin [38]. The peak observed at 1,600 cm^{-1} is related to aromatic C=C and C=O of conjugated ketones and quinones, and an increase in the intensity of this region increases the degree of condensation of aromatic organic compounds [39]. The peak at 1,705 cm^{-1} also exists only in SAT-Raw, indicating carbonyl groups in ester and ring structures [40]. In SAT-Raw, characteristic peaks of cellulose and hemicellulose corresponding to polysaccharides appear at 1,000–1,200 cm^{-1}, which lose their strength with increasing pyrolysis temperature [41]. As pyrolysis proceeds, a peak at 1,630 cm^{-1} is typically observed, which is attributed to C=C stretching vibration and is due to the presence of aromatic C=C bonds or C=O ring stretching [42,43]. After pyrolysis, a peak at approximately 1,200 cm^{-1} was observed, and the peak present in this vicinity was oscillated by C–O, which exists in carbon oxides such as acids, alcohols, ethers, or esters [44]. The peaks between 870 and 600 cm^{-1} are associated with C–Cl, and are typically detected at higher pyrolysis temperatures [45]. A peak at 3,600 cm^{-1} is clearly observed in SAT-300, and a peak around this region indicates the presence of hydroxyl groups [46], which is consistent with the high H content of SAT-300.

Fig. 2b shows the thermogravimetric (TG) and differential thermogravimetric (DTG) curves of the *A. turbinata* seed shells obtained from TGA. The TG and DTG curve plots revealed thermal degradation at distinct regions. The weight loss in the region below 200°C occurred because of the evaporation of the moisture content bound to the seed shell [47]. The highest rate of weight loss of 64.9% occurred in the range of 200°C–400°C, during which most volatile substances were extracted from the sample [48]. In this process, hemicellulose and cellulose were decomposed [49]. At temperatures above 400°C, weight was gradually reduced owing to lignin decomposition [48].

3.2. Effect of pyrolysis temperature on the triclosan adsorption of A. turbinata seed shell-derived biochar

The influence of pyrolysis temperature on the triclosan adsorption capacity of SAT-Raw and SAT-BC pyrolyzed at different temperatures was investigated. Fig. 3 shows the adsorption results for each pyrolysis temperature, indicating that SAT-300 exhibited the highest adsorption capacity, with robust interaction with triclosan. SAT-Raw adsorbed 21.5 mg/g of triclosan, which increased to 31.4 mg/g when the pyrolysis temperature was 300°C.

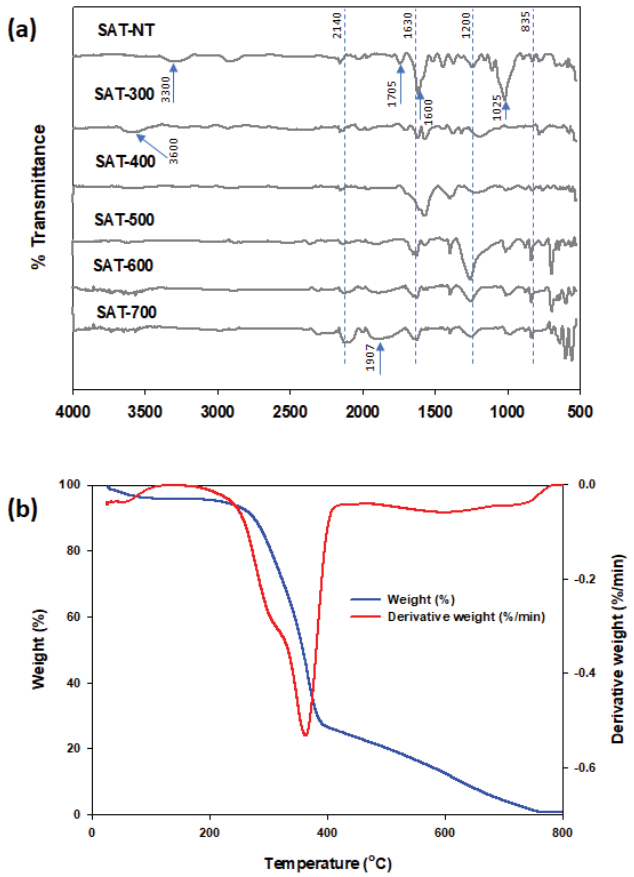

Fig. 2. (a) FTIR spectra of biochar derived from *Aesculus turbinata* seed shell at different temperatures (non-treated, 300°C, 400°C, 500°C, 600°C, and 700°C) and (b) thermogram and differential thermogram obtained via thermogravimetric analysis of *Aesculus turbinata* seed shell between 30°C and 800°C.

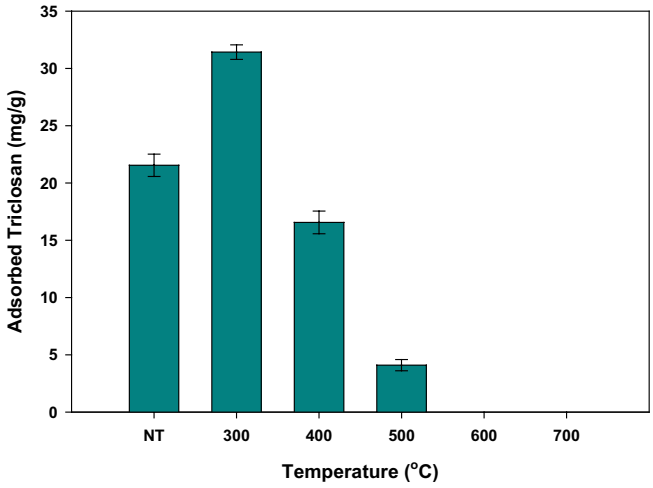

Fig. 3. Effect of pyrolysis temperature on the triclosan adsorption capacity of *Aesculus turbinata* seed shell-derived biochar (initial triclosan concentration: 100 mg/L; adsorbent dose: 1.67 g/L; reaction time: 24 h; reaction temperature: 25°C; agitation speed: 100 rpm).

SAT-300 exhibited the highest adsorption capacity, and SAT-BC pyrolyzed at temperatures higher than 300°C presented a lower adsorption ability than that of SAT-300. This indicates that extremely high pyrolysis temperature inhibits the triclosan adsorption by *A. turbinata* seed shell. This result is consistent with the results of previous studies indicating that the pyrolysis temperature and adsorption amount are inversely proportional [50,51]. Biochar produced at low temperatures has acidic characteristics due to the loss of volatile compounds, resulting in the adsorption of deprotonated acidic organic molecules, such as triclosan [50,52]. The increase in pyrolysis temperature from 300°C to 700°C decreased the O/C and H/C of SAT-BC, indicating that the change in chemical composition affected the triclosan adsorption capacity of SAT-BC. In SAT-300, a distinct hydroxyl group exists, which forms a hydrogen bond with triclosan. Similar hydrogen bonding between triclosan and metal-organic-framework adsorbent has also been reported in other literature [53]. The high solubility of triclosan was observed in the solvents with proton-acceptor functional groups because of the strong hydrogen bonding between triclosan and the solvents [54].

3.3. Adsorption kinetics

The kinetic adsorption experiment for SAT-300, which exhibited the highest triclosan adsorption capacity, was conducted by varying the reaction time. The obtained results were analyzed using kinetic adsorption models, including pseudo-first-order, pseudo-second-order, and intraparticle diffusion models, and the resulting parameters are listed in Table 2. Adsorption kinetic studies provide comprehensive information, such as the adsorption rates, adsorbent performance, and mass transfer mechanisms [55]. As shown in Fig. 4a, triclosan adsorption amounts rapidly increased in the initial stages and then gradually increased to reach

Table 2
Parameters of kinetic models obtained by fitting the model to triclosan adsorption data using SAT-300 at different reaction times

Pseudo-first-order kinetic model parameters				Pseudo-second-order kinetic model parameters				Intraparticle diffusion kinetic model parameters	
q_e (mg/g)	k_1 (h^{-1})	R^2	SEE	q_e (mg/g)	k_2 (g/(mg·h))	R^2	SEE	K_p ((mg/g)·$h^{1/2}$)	R^2
31.8	8.25	0.968	2.17	32.9	0.56	0.983	1.58	2.51 0.99	0.935 0.999

q_e: the amount of triclosan adsorbed onto SAT-300 at equilibrium (mg/g); k_1: the rate constant of pseudo-first-order adsorption (h^{-1}); k_2: the rate constant of pseudo-second-order adsorption (g/(mg·h)); K_p: the intraparticle diffusion rate constant ((mg/g)·$h^{1/2}$).

equilibrium within 6 h. The pseudo-second-order model presented a regression coefficient (R^2) value of 0.983, with lower sum of squared error (SEE) values, indicating a better correlation coefficient when compared to that of the pseudo-first-order model (R^2 = 0.968). The q_e value obtained from pseudo-second-order modeling was 32.9 mg/g, which was similar to the q_e value of 34.9 mg/g obtained through the experiment. These results imply that the pseudo-second-order model suitably described triclosan adsorption kinetics by SAT-300 rather than that of the pseudo-first-order model, which indicates that the triclosan adsorption rate by SAT-300 primarily depends on chemisorption [56].

Fig. 4b shows an analysis of the adsorption kinetics using the intraparticle diffusion model. The intraparticle diffusion models can explain the diffusion control process of triclosan adsorption by SAT-300. This model is expressed as a function of the amount of triclosan adsorbed (mg/g) and the square root of time ($h^{1/2}$), and its parameters are listed in Table 2. The diffusion rate constant of particles, which represents the adsorption rate, is k_i and is expressed as the slope value of the model [57]. The constant value of the equation determines whether the line graph passes through the origin. A previous study showed that when the intraparticle diffusion is the rate-controlling factor, the amount of adsorption depends on the square root of time, and when the plot does not pass through the origin, intraparticle diffusion is not the only rate-controlling factor [58]. In this study, the linear graph did not pass through the origin, which implied that pore diffusion was not the only rate-controlling factor in triclosan adsorption [59]. The first part of the line graph represents the diffusion process controlled by the outer surface, and the second part represents the diffusion within the particle [60].

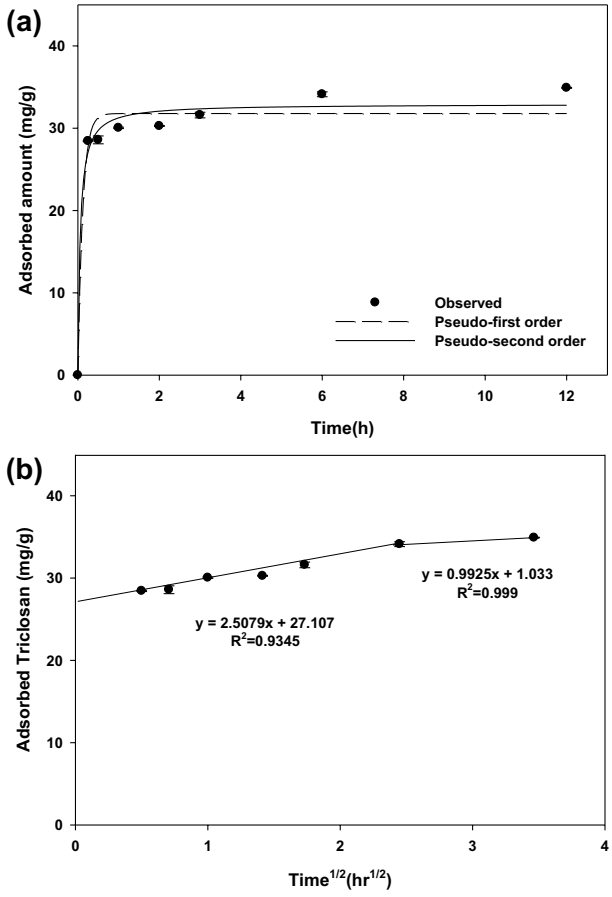

Fig. 4. (a) Kinetic adsorption results for triclosan adsorption by SAT-300 and model fit using pseudo-first-order and pseudo-second-order models and (b) intraparticle diffusion model fitted to kinetic adsorption data (time$^{1/2}$ vs. adsorbed triclosan) (initial triclosan concentration: 100 mg/L; adsorbent dose: 1.67 g/L; reaction time: 0.25–12 h; reaction temperature: 25°C; agitation speed: 100 rpm).

3.4. Adsorption isotherm

The adsorption equilibrium of triclosan by SAT-300 was analyzed by varying the initial concentrations of triclosan (5–100 mg/L), and the results are plotted in Fig. 5. Isotherm adsorption is a primary technique for determining the distribution of the adsorbate between the liquid and solid phases, and the adsorption capacity of the adsorbent [61,62]. Table 3 lists the Langmuir and Freundlich isotherm parameters for adsorption. The applied Freundlich model presented

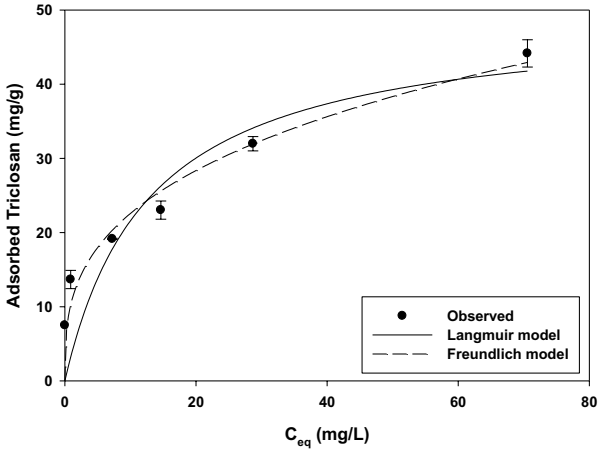

Fig. 5. Adsorption isotherm data for triclosan adsorption by SAT-300 and model fitting using Langmuir and Freundlich models (initial triclosan concentration: 5–100 mg/L; adsorbent dose: 0.67 g/L; reaction time: 12 h; reaction temperature: 25°C; agitation speed: 100 rpm).

Table 3
Parameter of kinetic models obtained by fitting the model to the adsorption of triclosan on SAT-300 under different triclosan concentration in aqueous phases at equilibrium

Model	Parameters		R^2	SEE
Langmuir	Q_m (mg/g)	K_L (L/mg)	0.783	6.869
	49.4	0.078		
Freundlich	K_F ((mg/g)·(L/mg)$^{1/n}$)	$1/n$	0.911	4.412
	10.6	0.803		

Q_m: the maximum adsorption capacity of triclosan per unit mass of SAT-300 (mg/g); K_L: Langmuir constant related to the binding energy (L/mg); K_F: distribution coefficient ((mg/g)·(L/mg)$^{1/n}$); n: Freundlich constant.

a regression coefficient (R^2) value of 0.911, indicating that the experimental adsorption data fit well with the Freundlich model. The Freundlich isotherm describes reversible adsorption and is a model applicable to multilayer adsorption [63]; hence, it can be inferred that triclosan adsorption by SAT-300 proceeds in the form of multilayer adsorption. In the Freundlich model, the affinity of the adsorption type is expressed as $1/n$, where n is a constant representing the adsorption strength [64]. The $1/n$ value is also a measure of adsorption intensity or surface heterogeneity, and the closer the value is to 0, the higher is the heterogeneity [65]. In this study, the $1/n$ value was 0.803, indicating normal adsorption ($1/n < 1$: normal adsorption; $1/n > 1$: cooperative adsorption) [66]. The K_F value, distribution coefficient indicating the amount of adsorbate adsorbed to the adsorbent per unit equilibrium concentration [65], is 10.6 $(mg/g)\cdot(L/mg)^{1/n}$.

The maximum amount adsorbed by SAT-300 obtained from the Langmuir model was 49.4 mg/g, which is similar to that obtained from the experimental data (44.2 mg/g). The triclosan adsorption capacity for commercial activated carbon was 41.2 mg/g [13], and SAT-300 displayed a higher adsorption capacity than that of the activated carbon. The maximum adsorption capacity of triclosan by various types of adsorbents investigated in other studies is shown in Table 4, and the adsorption capacity of SAT-300 was comparable with that of the other adsorbents. SAT-300 is an adsorbent obtained from *A. turbinata* seed shell, a street tree, which is relatively easy to access. The cost for the thermal treatment of *A. turbinata* seed shell at 300°C was calculated by considering the consumed electricity. For treating 15 g of *A. turbinata* seed shell, 1.8 kW h of electricity is consumed, and its cost is 109 KRW. From TGA analysis, the recovery of *A. turbinata* seed shell at 300°C for 1 h was 81.6%. The 147.1 kW h of electricity per 1 kg of SAT-300 was consumed, and it corresponded to 8,907 KRW (=7.07 USD). The production cost for SAT-300 can be reduced through the large-scale pyrolysis process, and the gas generated during the production process also can partially compensate for the price.

3.5. Adsorption thermodynamic parameters

The transfer of moles of solute units to the solid–liquid interface changes the enthalpy ($\Delta H°$), entropy ($\Delta S°$), and free energy ($\Delta G°$). Therefore, these parameters are important factors to consider when determining the adsorption process. The adsorption of triclosan onto SAT-300 was quantified using Eqs. (6)–(9) and the thermodynamic parameters are presented in Table 5. The enthalpy ($\Delta H°$) quantified through triclosan adsorption using SAT-300 has a positive value, indicating that the adsorption process is endothermic. An increase in the reaction temperature decreases the viscosity of the solution, causing an increase in the diffusion rate of the adsorbed water molecules across the outer boundary layer of the adsorbent particles and the inner pores [78]. Increasing the temperature improves the mobility of the adsorbed molecules, thereby increasing the adsorption amount [79]. An enthalpy change ($\Delta H°$) of less than 20 kJ/mol indicates physical adsorption, whereas a value between 80 and 200 kJ/mol indicates chemical adsorption [80]. The enthalpy change ($\Delta H°$) for triclosan adsorbed by SAT-300 is 22.2 kJ/mol, indicating that the adsorption occurs at the boundary between physical and chemical adsorption. The positive entropy

Table 4
Maximum adsorption capacity of triclosan by various types of adsorbents

Adsorbent	Adsorption capacity (mg-triclosan/g)	Initial concentration (mg/L)	Reaction time (h)	Temperature (°C)	Size (mm)	pH	Reference
Optimized activated carbon	117.0	25–500	4	25	0.25–0.425	6.9	[67]
Char derived from palm kernel shell	88.9	1–500	24	25	0.85–1.18	–	[68]
Biochar derived from kenaf	77.4	5–160	24	25	0.5	6.3	[69]
Thermally treated rice husk	72.7	1–400	6	25	0.50–0.15	–	[70]
Tyre crumb rubber	62.5	10–60	24	25	0.67	7	[71]
Biochar from seed shell of *Aesculus turbinata* (SAT-300)	49.4	5–100	12	25		6.5	This study
Charcoal-based activated carbon	41.2	10–60	24	25	1.5	3	[13]
Polyvinyl chloride	40.2	2–20	24	25	0.074		[72]
Activated carbon derived from waste biomass (coconut pulp waste)	38.9	10–90	1	25	0.6	5.6	[73]
Single-walled carbon nanotubes	33.0	1–50	24	25		7	[74]
Organo-zeolites	31.9	0–50	10	25	0.075	6.7	[10]
Kaolinite	22.0	10–60	24	25	0.006	3	[13]
Biomass of *Phaeodactylum tricornutum*	13.0	1–50	3	18	–	7	[75]
Commercial Activated carbon	3.5	0.025–1	4	25	–	6.7	[76]
Carbon nanotubes imprinted polymers	0.8–1.8	0–0.04	3	–	0.005–0.015	–	[77]
Wastewater biosolids-derived biochar	0.87	0–0.02	24	–	–	6.5	[17]

Table 5
Enthalpy, entropy, and Gibb's free energy for the adsorption of triclosan by SAT-300

Temperature	$\Delta H°$	$\Delta S°$	$\Delta G°$
(°C)	(kJ/mol)	(J/K·mol)	(kJ/mol)
15	22.2	67.9	2.60
25	–	–	1.92
35	–	–	1.24

Initial triclosan concentration: 100 mg/L; adsorbent dose: 1.67 g/L; reaction time: 12 h; reaction temperature: 15°C, 25°C and 35°C; agitation speed: 100 rpm.

($\Delta S°$) value suggested an increasing randomness at the solid–liquid interface during the adsorption process of triclosan onto the active sites of SAT-300. The translation entropy of the displaced water molecule is higher than that of the water molecule lost due to triclosan adsorption, which increases the randomness at the solid–liquid interface [81]. The complex is excited during the transition state and the free energy ($\Delta G°$) value is positive, indicating the presence of an energy barrier during the adsorption process [82]. Furthermore, small but positive values of free energy also indicate that the adsorption process requires additional energy [83].

3.6. Effect of pH on the adsorption of triclosan

pH value is one of the factors affecting the adsorption of pollutants in water. A change in pH causes protonation or deprotonation of functional groups on the surface of the adsorbent and adsorbate, thereby affecting the charge and causing electrostatic attraction or repulsion between them [84,85]. Fig. 6 shows the effect of pH on triclosan adsorption by SAT-300. An increase in pH value from 3 to 7 decreases the triclosan adsorption amount from 33.0 to 23.5 mg/g; when the pH values increased from 7 to 11, the adsorption amount sharply decreased from 23.5 to 7.4 mg/g.

This is consistent with the results of previous studies indicating the decrease in triclosan adsorption with the increase in the solution pH [72,86]. Generally, an increase in solution pH results in completely deprotonated surface functional groups, which is one of the reasons for the loss of positive charge and accumulation of negative charge [87]. The pH of the solution affected the dissociation of triclosan; pK_a is the triclosan dissociation marginal point and triclosan is undissociated under acidic conditions below its dissociation constant (pK_a = 8.14). The charge of the undissociated triclosan is neutral, which minimizes electrostatic repulsion and improves adsorption ability [13]. When the net charge of the adsorbent is negative, the amount adsorbed increases as the interaction of repulsive static electricity is minimized [13]. In Fig. 6, triclosan adsorption onto SAT-300 sharply decreased from 23.5 to 14.6 mg/g as the initial pH changed from 7 to 9. This is because triclosan dissociated and converted into a negative ion when the final solution pH increased to above 8.5. At higher pH, the surface charge of the adsorbent becomes significantly negative, thereby increasing the repulsive force between both the negatively charged molecule and the adsorbent [88]. At pH values higher than

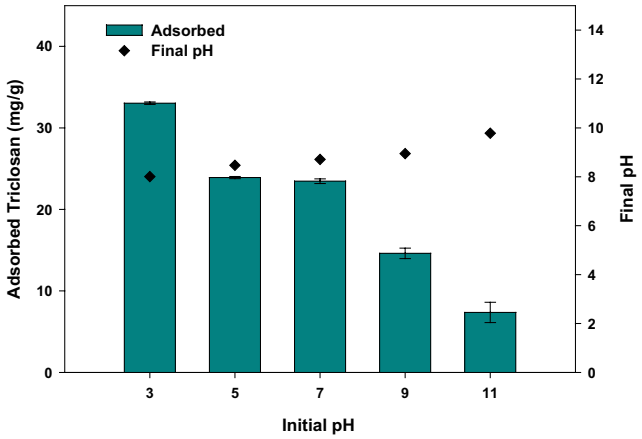

Fig. 6. Effects of solution pH on the adsorption of triclosan by SAT-300 (initial triclosan concentration: 100 mg/L; adsorbent dose: 1.67 g/L; initial pH: 3–11; reaction time: 12 h; reaction temperature: 25°C; agitation speed: 100 rpm).

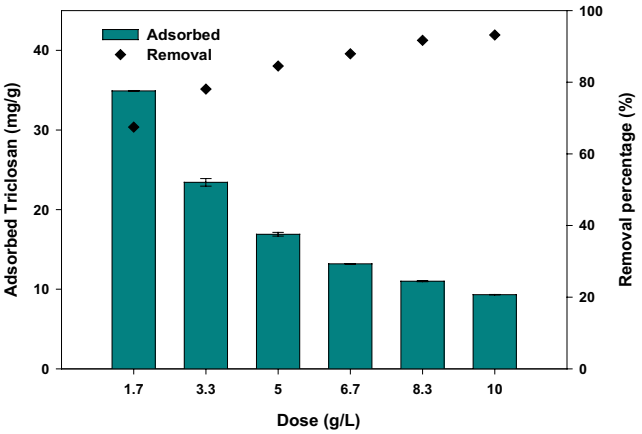

Fig. 7. Effects of SAT-300 dose on its adsorption capacity and triclosan removal percentage (initial triclosan concentration: 100 mg/L; adsorbent dose: 1.67–10 g/L; reaction time: 12 h; reaction temperature: 25°C; agitation speed: 100 rpm).

pK_a, the total surface charge of the adsorbent becomes negative, and triclosan in the anionic form dominates in the solution.

3.7. Effect of adsorbent dosage on the adsorption of triclosan

Fig. 7 presents the adsorption amount of triclosan according to the concentration of SAT-300 (1.7–10.0 g/L). An increase in the SAT-300 dose from 1.7 to 10.0 g/L steadily decreased the adsorption amount from 34.9 to 9.3 mg/g, while the removal efficiency increased from 67.5% to 93.2%. The triclosan removal efficiency increased with the dose of SAT-300 within a fixed initial concentration due to more adsorption sites. A dosage of 8.3 g/L is required to remove more than 90% of triclosan. Previous studies have shown that increasing the adsorbent dosage can provide additional binding sites for triclosan adsorption, while excess adsorbent dose may not be completely utilized during adsorption [89,90].

4. Conclusion

Triclosan, an antimicrobial agent widely used in personal care products, was removed using biochar derived from the seed shell of *A. turbinata*, and the SAT-BC application for TCS removal had never been tried by others researchers. The biochar was pyrolyzed at different temperatures (300°C–700°C), and their physico-chemical properties and triclosan adsorption amounts were quantified. An increase in pyrolysis temperature decreased the O/C and H/C of SAT-BC, indicating the reduced hydrophilicity and increased aromaticity of SAT-BC. The SAT-300 with the highest O/C and H/C exhibited the highest triclosan adsorption capacity because of strong hydrogen bonding between triclosan and SAT-300. The rate of triclosan adsorption by SAT-300 was mainly governed by chemisorption. Freundlich model suitably described triclosan adsorption than that of the Langmuir model, indicating that triclosan was adsorbed onto the homogeneous surface of SAT-300 via a multilayer. The maximum adsorption capacity of SAT-300 was 49.4 mg/g, which is comparable to that of other adsorbents reported in the literature. The enthalpy change of triclosan adsorption by SAT-300 was 22.2 kJ/mol, which ranged between the boundary of physical and chemical adsorption. Triclosan adsorption was reduced sharply at an initial solution pH between 7 and 9 because of the dissociation of triclosan molecules, leading to the increased electrostatic repulsion between dissociated triclosan and the negatively charged surface of SAT-300. The increase in the SAT-300 dose increased the triclosan removal percentage, but reduced the amount of triclosan adsorption per unit mass of the adsorbent. This study suggested that the biochar derived from the biowaste of seed shells could be utilized as a valuable adsorbent for removing triclosan from an aqueous solution.

References

[1] R.D. Jones, H.B. Jampani, J.L. Newman, A.S. Lee, Triclosan: a review of effectiveness and safety in health care settings, Am. J. Infect. Control., 28 (2000) 184–196.

[2] A.B. Dann, A. Hontela, Triclosan: environmental exposure, toxicity and mechanisms of action, J. Appl. Toxicol., 31 (2011) 285–311.

[3] I. Aguilar-Romero, E. Romero, R.-M. Wittich, P. van Dillewijn, Bacterial ecotoxicity and shifts in bacterial communities associated with the removal of ibuprofen, diclofenac and triclosan in biopurification systems, Sci. Total Environ., 741 (2020) 140461, doi: 10.1016/j.scitotenv.2020.140461.

[4] S. Lu, N. Wang, S. Ma, X. Hu, L. Kang, Y. Yu, Parabens and triclosan in shellfish from Shenzhen coastal waters: bioindication of pollution and human health risks, Environ. Pollut., 246 (2019) 257–263.

[5] G.S. Dhillon, S. Kaur, R. Pulicharla, S.K. Brar, M. Cledón, M. Verma, R.Y. Surampalli, Triclosan: current status, occurrence, environmental risks and bioaccumulation potential, Int. J. Environ. Res. Public Health, 12 (2015) 5657–5684.

[6] D.R. Orvos, D.J. Versteeg, J. Inauen, M. Capdevielle, A. Rothenstein, V. Cunningham, Aquatic toxicity of triclosan, Environ. Toxicol. Chem., 21 (2002) 1338–1349.

[7] A. Thompson, P. Griffin, R. Stuetz, E. Cartmell, The fate and removal of triclosan during wastewater treatment, Water Environ. Res., 77 (2005) 63–67.

[8] Z. Luo, Y. He, D. Zhi, L. Luo, Y. Sun, E. Khan, D.C. Tsang, Current progress in treatment techniques of triclosan from wastewater: a review, Sci. Total Environ., 696 (2019) 133990, doi: 10.1016/j.scitotenv.2019.133990.

[9] T.A. Saleh, Protocols for synthesis of nanomaterials, polymers, and green materials as adsorbents for water treatment technologies, Environ. Technol. Innovation, 24 (2021) 101821, doi: 10.1016/j.eti.2021.101821.

[10] C. Lei, Y.Y. Hu, M.Z. He, Adsorption characteristics of triclosan from aqueous solution onto cetylpyridinium bromide (CPB) modified zeolites, Chem. Eng. J., 219 (2013) 361–370.

[11] T.A. Saleh, M. Mustaqeem, M. Khaled, Developing water treatment technologies in removing heavy metals from wastewater: a review, Environ. Nanotechnol. Monit. Manage., 17 (2022) 100617, doi: 10.1016/j.enmm.2021.100617.

[12] M. Kim, J. Lee, C. Lee, S. Park, Thermal treatment of attapulgite for phosphate removal: a cheap and natural adsorbent with high adsorption capacity, Desal. Water Treat., 114 (2018) 175–184.

[13] S.K. Behera, S.Y. Oh, H.S. Park, Sorption of triclosan onto activated carbon, kaolinite and montmorillonite: effects of pH, ionic strength, and humic acid, J. Hazard. Mater., 179 (2010) 684–691.

[14] H.H. Cho, H. Huang, K. Schwab, Effects of solution chemistry on the adsorption of ibuprofen and triclosan onto carbon nanotubes, Langmuir, 27 (2011) 12960–12967.

[15] A. Dąbrowski, P. Podkościelny, Z. Hubicki, M. Barczak, Adsorption of phenolic compounds by activated carbon—a critical review, Chemosphere, 58 (2005) 1049–1070.

[16] L. Li, P.A. Quinlivan, D.R. Knappe, Effects of activated carbon surface chemistry and pore structure on the adsorption of organic contaminants from aqueous solution, Carbon, 40 (2002) 2085–2100.

[17] Y. Tong, B.K. Mayer, P.J. McNamara, Triclosan adsorption using wastewater biosolids-derived biochar, Environ. Sci. Water Res. Technol., 2 (2016) 761–768.

[18] H. Bamdad, K. Hawboldt, S. MacQuarrie, A review on common adsorbents for acid gases removal: focus on biochar, Renewable Sustainable Energy Rev., 81 (2018) 1705–1720.

[19] M. Ahmad, A.U. Rajapaksha, J.E. Lim, M. Zhang, N. Bolan, D. Mohan, Y.S. Ok, Biochar as a sorbent for contaminant management in soil and water: a review, Chemosphere, 99 (2014) 19–33.

[20] J. Li, Y. Li, Y. Wu, M. Zheng, A comparison of biochars from lignin, cellulose and wood as the sorbent to an aromatic pollutant, J. Hazard. Mater., 280 (2014) 450–457.

[21] P.J.M. Carrott, M.R. Carrott, Lignin–from natural adsorbent to activated carbon: a review, Bioresource Technol., 98 (2007) 2301–2312.

[22] Y. Li, S.M. Shaheen, J. Rinklebe, N.L. Ma, Y. Yang, M.A. Ashraf, W.X. Peng, Pyrolysis of *Aesculus chinensis* Bunge seed with Fe_2O_3/NiO as nanocatalysts for the production of bio-oil material, J. Hazard. Mater., 416 (2021) 126012, doi: 10.1016/j.jhazmat.2021.126012.

[23] L.R. Drăghici, D.I. Hădărugă, N.G. Hădărugă, Aesculus species: a review on biologically active compounds and their possible applications, J. Agroaliment. Proc. Technol., 26 (2020) 422–428.

[24] H. Kimura, S. Ogawa, A. Sugiyama, M. Jisaka, T. Takeuchi, K. Yokota, Anti-obesity effects of highly polymeric proanthocyanidins from seed shells of Japanese horse chestnut (*Aesculus turbinata* Blume), Food Res. Int., 44 (2011) 121–126.

[25] H. Kimura, S. Ogawa, T. Ishihara, M. Maruoka, S. Tokuyama-Nakai, M. Jisaka, K. Yokota, Antioxidant activities and structural characterization of flavonol O-glycosides from seeds of Japanese horse chestnut (*Aesculus turbinata* BLUME), Food Chem., 228 (2017) 348–355.

[26] J.C. Carlson, M.I. Stefan, J.M. Parnis, C.D. Metcalfe, Direct UV photolysis of selected pharmaceuticals, personal care products and endocrine disruptors in aqueous solution, Water Res., 84 (2015) 350–361.

[27] L. Shi, X. Zho, S. Zhou, Y. Zhang, Adsorption Isotherm and Thermodynamic of Triclosan on Activated Sludge, International Conference on Electric Technology and Civil Engineering., IEEE, Lushan, China, 2011, pp. 975–978.

[28] A.A. Sharipova, S.B. Aidarova, N.E. Bekturganova, A. Tleuova, M. Schenderlein, O. Lygina, R. Miller, Triclosan as model system

for the adsorption on recycled adsorbent materials, Colloids Surf., A, 505 (2016) 193–196.
[29] M. He, Z. Xu, Y. Sun, P.S. Chan, I. Lui, D.C.W. Tsang, Critical impacts of pyrolysis conditions and activation methods on application-oriented production of wood waste-derived biochar, Bioresour. Technol., 341 (2021) 125811, doi: 10.1016/j.biortech.2021.125811.
[30] L.M. Machado, S.F. Lütke, D. Perondi, M. Godinho, M.L. Oliveira, G.C. Collazzo, G.L. Dotto, Simultaneous production of mesoporous biochar and palmitic acid by pyrolysis of brewing industry wastes, Waste Manage., 113 (2020) 96–104.
[31] J. Rouquerol, D. Avnir, C.W. Fairbridge, D.H. Everett, J.M. Haynes, N. Pernicone, K.K. Unger, Recommendations for the characterization of porous solids (Technical Report), Pure Appl. Chem., 66 (1994) 1739–1758.
[32] K. Zhu, X. Wang, M. Geng, D. Chen, H. Lin, H. Zhang, Catalytic oxidation of clofibric acid by peroxydisulfate activated with wood-based biochar: effect of biochar pyrolysis temperature, performance and mechanism, Chem. Eng. J., 374 (2019) 1253–1263.
[33] K.H. Kim, J.Y. Kim, T.S. Cho, J.W. Choi, Influence of pyrolysis temperature on physico-chemical properties of biochar obtained from the fast pyrolysis of pitch pine (*Pinus rigida*), Bioresour. Technol., 118 (2012) 158–162.
[34] D. Chen, X. Yu, C. Song, X. Pang, J. Huang, Y. Li, Effect of pyrolysis temperature on the chemical oxidation stability of bamboo biochar, Bioresour. Technol., 218 (2016) 1303–1306.
[35] W.A.W.A.K. Ghani, A. Mohd, G. da Silva, R.T. Bachmann, Y.H. Taufiq-Yap, U. Rashid, A.H. Al-Muhtaseb, Biochar production from waste rubber-wood-sawdust and its potential use in C sequestration: chemical and physical characterization, Ind. Crops Prod., 44 (2013) 18–24.
[36] Y. Jia, S. Shi, J. Liu, S. Su, Q. Liang, X. Zeng, T. Li, Study of the effect of pyrolysis temperature on the Cd^{2+} adsorption characteristics of biochar, Appl. Sci., 8 (2018) 1019, doi: 10.3390/app8071019.
[37] B. Khiari, I. Ghouma, A.I. Ferjani, A.A. Azzaz, S. Jellali, L. Limousy, M. Jeguirim, Kenaf stems: thermal characterization and conversion for biofuel and biochar production, Fuel, 262 (2020) 116654, doi: 10.1016/j.fuel.2019.116654.
[38] K.B. Cantrell, P.G. Hunt, M. Uchimiya, J.M. Novak, K.S. Ro, Impact of pyrolysis temperature and manure source on physicochemical characteristics of biochar, Bioresour. Technol., 107 (2012) 419–428.
[39] B. Zhao, D. O'Connor, J. Zhang, T. Peng, Z. Shen, D.C. Tsang, D. Hou, Effect of pyrolysis temperature, heating rate, and residence time on rapeseed stem derived biochar, J. Cleaner Prod., 174 (2018) 977–987.
[40] T.A. Saleh, The influence of treatment temperature on the acidity of MWCNT oxidized by HNO_3 or a mixture of HNO_3/H_2SO_4, Appl. Surf. Sci., 257 (2011) 7746–7751.
[41] C. Trigo, L. Cox, K. Spokas, Influence of pyrolysis temperature and hardwood species on resulting biochar properties and their effect on azimsulfuron sorption as compared to other sorbents, Sci. Total Environ., 566 (2016) 1454–1464.
[42] J. Gao, Y. Liu, X. Li, M. Yang, J. Wang, Y. Chen, A promising and cost-effective biochar adsorbent derived from jujube pit for the removal of Pb(II) from aqueous solution, Sci. Rep., 10 (2020) 1–13.
[43] B.B. Kaudal, D. Chen, D.B. Madhavan, A. Downie, A. Weatherley, An examination of physical and chemical properties of urban biochar for use as growing media substrate, Biomass Bioenergy, 84 (2016) 49–58.
[44] H. Zeng, H. Zeng, H. Zhang, A. Shahab, K. Zhang, Y. Lu, I. Nabi, F. Naseem, H. Ullah, Efficient adsorption of Cr(VI) from aqueous environments by phosphoric acid activated eucalyptus biochar, J. Cleaner Prod., 286 (2021) 124964, doi: 10.1016/j.jclepro.2020.124964.
[45] W.W. Simons, The Sadtler Handbook of Infrared Spectra, Sadtler Research Laboratories, Philadelphia, 1978.
[46] V. Sharma, S. Bhardwaj, R. Kumar, On the spectroscopic investigation of Kohl stains via ATR-FTIR and multivariate analysis: application in forensic trace evidence, Vib. Spectrosc., 101 (2019) 81–91.
[47] P. Kumar, P. Kumar, P.V. Rao, N.V. Choudary, G. Sriganesh, Saw dust pyrolysis: effect of temperature and catalysts, Fuel, 199 (2017) 339–345.
[48] B. Soni, S.K. Karmee, Towards a continuous pilot scale pyrolysis based biorefinery for production of biooil and biochar from sawdust, Fuel, 271 (2020) 117570, doi: 10.1016/j.fuel.2020.117570.
[49] U. Moralı, S. Şensöz, Pyrolysis of hornbeam shell (*Carpinus betulus* L.) in a fixed bed reactor: characterization of bio-oil and bio-char, Fuel, 150 (2015) 672–678.
[50] B. Czech, M. Kończak, M. Rakowska, P. Oleszczuk, Engineered biochars from organic wastes for the adsorption of diclofenac, naproxen and triclosan from water systems, J. Cleaner Prod., 288 (2021) 125686, doi: 10.1016/j.jclepro.2020.125686.
[51] S.Y. Oh, Y.D Seo, Sorption of halogenated phenols and pharmaceuticals to biochar: affecting factors and mechanisms, Environ. Sci. Pollut. Res., 23 (2016) 951–961.
[52] I. Kozyatnyk, P. Oesterle, C. Wurzer, O. Mašek, S. Jansson, Removal of contaminants of emerging concern from multicomponent systems using carbon dioxide activated biochar from lignocellulosic feedstocks, Bioresour. Technol., 340 (2021) 125561, doi: 10.1016/j.biortech.2021.125561.
[53] M. Yang, P. Guo, X. Feng, W. Zhang, G. Yang, Solid solution approach to the design of copper mixed-triazolate multivariate-MOFs for the efficient adsorption of triclosan, Microporous Mesoporous Mater., 324 (2021) 111297, doi: 10.1016/j.micromeso.2021.111297.
[54] D.M. Aragón, M.A. Ruidiaz, E.F. Vargas, C. Bregni, D.A. Chiappetta, A. Sosnik, F. Martínez, Solubility of the antimicrobial agent triclosan in organic solvents of different hydrogen bonding capabilities at several temperatures, J. Chem. Eng. Data, 53 (2008) 2576–2580.
[55] J. Wang, X. Guo, Adsorption kinetic models: physical meanings, applications, and solving methods, J. Hazard. Mater., 390 (2020) 122156, doi: 10.1016/j.jhazmat.2020.122156.
[56] H. Li, W. Zhang, Z. Zhang, X. Zhang, Sorption of triclosan to carbon nanotubes: the combined effects of sonication, functionalization and solution chemistry, Sci. Total Environ., 580 (2017) 1318–1326.
[57] A.W. Ip, J.P. Barford, G. McKay, A comparative study on the kinetics and mechanisms of removal of Reactive Black 5 by adsorption onto activated carbons and bone char, Chem. Eng. J., 157 (2010) 434–442.
[58] Z. Cheng, X. Liu, M. Han, W. Ma, Adsorption kinetic character of copper ions onto a modified chitosan transparent thin membrane from aqueous solution, J. Hazard. Mater., 182 (2010) 408–415.
[59] K. Mohanty, M. Jha, B.C. Meikap, M.N. Biswas, Preparation and characterization of activated carbons from *Terminalia arjuna* nut with zinc chloride activation for the removal of phenol from wastewater, Ind. Eng. Chem. Res., 44 (2005) 4128–4138.
[60] S.K. Singh, T.G. Townsend, D. Mazyck, T.H. Boyer, Equilibrium and intraparticle diffusion of stabilized landfill leachate onto micro-and meso-porous activated carbon, Water Res., 46 (2012) 491–499.
[61] R. Baccar, M. Sarrà, J. Bouzid, M. Feki, P. Blánquez, Removal of pharmaceutical compounds by activated carbon prepared from agricultural by-product, Chem. Eng. J., 211 (2012) 310–317.
[62] R. Wirasnita, T. Hadibarata, A.R.M. Yusoff, Z. Yusop, Removal of bisphenol A from aqueous solution by activated carbon derived from oil palm empty fruit bunch, Water Air Soil Pollut., 225 (2014) 1–12.
[63] K.Y. Foo, B.H. Hameed, Insights into the modeling of adsorption isotherm systems, Chem. Eng. J., 156 (2010) 2–10.
[64] S. Zhou, Y. Shao, N. Gao, J. Deng, C. Tan, Equilibrium, kinetic, and thermodynamic studies on the adsorption of triclosan onto multi-walled carbon nanotubes, Clean–Soil Air Water, 41 (2013) 539–547.
[65] N. Mohammadi, H. Khani, V.K. Gupta, E. Amereh, S. Agarwal, Adsorption process of methyl orange dye onto mesoporous

carbon material–kinetic and thermodynamic studies, J. Colloid Interface Sci., 362 (2011) 457–462.
[66] A.O. Dada, A.P. Olalekan, A.M. Olatunya, O.J.I.J.C. Dada, Langmuir, Freundlich, Temkin and Dubinin–Radushkevich isotherms studies of equilibrium sorption of Zn^{2+} unto phosphoric acid modified rice husk, IOSR. J. Appl. Chem., 3 (2012) 38–45.
[67] J.T. Yokoyama, A.L. Cazetta, K.C. Bedin, L. Spessato, J.M. Fonseca, P.S. Carraro, V.C. Almeida, Stevia residue as new precursor of CO_2-activated carbon: optimization of preparation condition and adsorption study of triclosan, Ecotoxicol. Environ. Saf., 172 (2019) 403–410.
[68] M. Triwiswara, C.G. Lee, J.K. Moon, S.J. Park, Adsorption of triclosan from aqueous solution onto char derived from palm kernel shell, Desal. Water Treat., 177 (2020a) 71–79.
[69] E.-J. Cho, J.-K. Kang, J.-K. Moon, B.-H. Um, C.-G. Lee, S.H. Jeong, S.-J. Park, Removal of triclosan from aqueous solution via adsorption by kenaf-derived biochar: its adsorption mechanism study via spectroscopic and experimental approaches, J. Environ. Chem. Eng., 9 (2021) 106343, doi: 10.1016/j.jece.2021.106343.
[70] M. Triwiswara, J.K. Kang, J.K. Moon, C.G. Lee, S.J. Park, Removal of triclosan from aqueous solution using thermally treated rice husks, Desal. Water Treat., 202 (2020b) 317–326.
[71] J. Lopez-Morales, O. Perales-Perez, F. Roman-Velazquez, Sorption of triclosan onto tyre crumb rubber, Adsorpt. Sci. Technol., 30 (2012) 831–845.
[72] J. Ma, J. Zhao, Z. Zhu, L. Li, F. Yu, Effect of microplastic size on the adsorption behavior and mechanism of triclosan on polyvinyl chloride, Environ. Pollut., 254 (2019) 113104, doi: 10.1016/j.envpol.2019.113104.
[73] N.K.E.M. Khori, T. Hadibarata, M.S. Elshikh, A.A. Al-Ghamdi, Z.Y. Salmiati, Z. Yusop, Triclosan removal by adsorption using activated carbon derived from waste biomass: isotherms and kinetic studies, J. Chin. Chem. Soc., 37 (2018) 1–9.
[74] L.A. González-Fernández, N.A. Medellín-Castillo, R. Ocampo-Pérez, H. Hernández-Mendoza, M.S. Berber-Mendoza, C. Aldama-Aguilera, Equilibrium and kinetic modelling of triclosan adsorption on single-walled carbon nanotubes, J. Environ. Chem. Eng., 9 (2021) 106382, doi: 10.1016/j.jece.2021.106382.
[75] S. Santaeufemia, J. Abalde, E. Torres, Eco-friendly rapid removal of triclosan from seawater using biomass of a microalgal species: kinetic and equilibrium studies, J. Hazard. Mater., 369 (2019) 674–683.
[76] F. Wang, X. Lu, W. Peng, Y. Deng, T. Zhang, Y. Hu, X.Y. Li, Sorption behavior of bisphenol A and triclosan by graphene: comparison with activated carbon, ACS. Omega, 2 (2017) 5378–5384.
[77] R. Gao, X. Kong, F. Su, X. He, L. Chen, Y. Zhang, Synthesis and evaluation of molecularly imprinted core–shell carbon nanotubes for the determination of triclosan in environmental water samples, J. Chromatogr. A, 1217 (2010) 8095–8102.
[78] I.A.W. Tan, A.L. Ahmad, B.H. Hameed, Adsorption isotherms, kinetics, thermodynamics and desorption studies of 2,4,6-trichlorophenol on oil palm empty fruit bunch-based activated carbon, J. Hazard. Mater., 164 (2009) 473–482.
[79] S. Senthilkumaar, P. Kalaamani, K. Porkodi, P.R. Varadarajan, C.V. Subburaam, Adsorption of dissolved reactive red dye from aqueous phase onto activated carbon prepared from agricultural waste, Bioresour. Technol., 97 (2006) 1618–1625.
[80] Q. Li, Q.Y. Yue, Y. Su, B.Y. Gao, H.J. Sun, Equilibrium, thermodynamics and process design to minimize adsorbent amount for the adsorption of acid dyes onto cationic polymer-loaded bentonite, Chem. Eng. J., 158 (2010) 489–497.
[81] A.A. Inyinbor, F.A. Adekola, G.A. Olatunji, Kinetics, isotherms and thermodynamic modeling of liquid phase adsorption of rhodamine B dye onto *Raphia hookerie* fruit epicarp, Water Resour. Ind., 15 (2016) 14–27.
[82] M. Alkan, Ö. Demirbaş, M. Doğan, Adsorption kinetics and thermodynamics of an anionic dye onto sepiolite, Microporous Mesoporous Mater., 101 (2007) 388–396.
[83] T. Wang, X. Jin, Z. Chen, M. Megharaj, R. Naidu, Simultaneous removal of Pb(II) and Cr(III) by magnetite nanoparticles using various synthesis conditions, J. Ind. Eng. Chem., 20 (2014) 3543–3549.
[84] Z. Feng, H. Chen, H. Li, R. Yuan, F. Wang, Z. Chen, B. Zhou, Preparation, characterization, and application of magnetic activated carbon for treatment of biologically treated papermaking wastewater, Sci. Total Environ., 713 (2020) 136423, doi: 10.1016/j.scitotenv.2019.136423.
[85] A. Ikhlaq, F. Javed, A. Niaz, H.M.S. Munir, F. Qi, Combined UV catalytic ozonation process on iron loaded peanut shell ash for the removal of methylene blue from aqueous solution, Desal. Water Treat., 200 (2020) 231–240.
[86] J.Y. Song, B.N. Bhadra, S.H. Jhung, Contribution of H-bond in adsorptive removal of pharmaceutical and personal care products from water using oxidized activated carbon, Microporous Mesoporous Mater., 243 (2017) 221–228.
[87] S.L. Wang, Y.M. Tzou, Y.H. Lu, G. Sheng, Removal of 3-chlorophenol from water using rice-straw-based carbon, J. Hazard. Mater., 147 (2007) 313–318.
[88] M.M.S. Saif, N.S. Kumar, M.N.V. Prasad, Binding of cadmium to *Strychnos potatorum* seed proteins in aqueous solution: adsorption kinetics and relevance to water purification, Colloids Surf., B, 94 (2012) 73–79.
[89] M. Ghorbani, H. Eisazadeh, A.A. Ghoreyshi, Removal of zinc ions from aqueous solution using polyaniline nanocomposite coated on rice husk, Iran. J. Energy Environ., 3 (2012) 83–88.
[90] M.A. Fard, A. Vosoogh, B. Barkdoll, B. Aminzadeh, Using polymer coated nanoparticles for adsorption of micropollutants from water, Colloids Surf., A, 531 (2017) 189–197.